Materials Advances

ROYAL SOCIETY OF CHEMISTRY

PAPER

View Article Online
View Journal | View Issue

Cite this: *Mater. Adv.*, 2025, 6, 2867

Side-chain engineering to develop phenyl-substituted benzodithiophenedione-unit-based polymer donors for efficient non-fullerene polymer solar cells†

Baitian He, ‡[a] WenZheng Zhang,‡[b] Jinming Zhang,[a] Yan Liu,*[a] Guiting Chen, *[a] Manjun Xiao*[b] and Chuanbo Dai[a]

Received 17th December 2024,
Accepted 11th March 2025

DOI: 10.1039/d4ma01259c

rsc.li/materials-advances

To improve the photovoltaic performance of non-fullerene polymer solar cells (NF-PSCs), it is essential to develop wide bandgap (WBG) polymer donors that can match with narrow bandgap non-fullerene acceptors. Side-chain engineering is a feasible strategy for designing efficient WBG polymer donors. This paper introduces two novel copolymers with linear alkyl chains (*n*-octyl) or branched alkyl chains (2-ethylhexyl) on the thiophene π-bridge. These copolymers incorporated a benzodithiophene (BDT) as the electron donor unit and a phenyl-substituted benzodithiophenedione (BDD-Ph) as the electron acceptor unit, with the resulting copolymers designated as PBF-C8 and PBF-EH, respectively. Compared with PBF-EH with branched side-chains, PBF-C8 with linear side-chains exhibited red-shifted absorption and stronger intermolecular aggregation. When paired with the narrow-bandgap non-fullerene acceptor L8-BO as the electron acceptor, the PBF-C8-based device achieved a power conversion efficiency of 16.44%, superior to that of the PBF-EH-based device (3.21%). This enhanced performance is attributable to the superior face-on orientation packing, exciton dissociation, and charge transport of the PBF-C8-based blended film. These findings indicate that using the BDD-Ph unit as the electron-deficient unit and optimising π-bridge side-chains can help construct highly efficient polymer donors.

Introduction

Bulk-heterojunction non-fullerene polymer solar cells (NF-PSCs) have attracted significant attention owing to their cost-effectiveness, mechanical flexibility, and low weight.[1–5] The efficiency of NF-PSCs has reached 19% with advancements in narrow-bandgap non-fullerene acceptors such as Y6 and its derivatives.[6–13] Recently, the Peng group demonstrated that pressure-controlled nanoimprint lithography fabrication of ordered interdigitated heterojunction structured OSCs achieves over 20% efficiency.[14] Chen's group developed the self-assembled interlayer (SAI) strategy to optimize the optical and electrical properties of OPVs, which results in a PCE exceeding 20%.[15] Improving the NF-PSC performance requires efficient wide-bandgap (WBG) polymer donors with complementary absorption spectra, matched energy levels, and suitable phase separation.[16–18] WBG polymer donors typically adopt a donor–π-bridge–acceptor (D–π–A) copolymer structure, enabling fine-tuning of the optical and electronic properties through photo-induced intramolecular charge transfer (ICT).[19–21] Incorporating suitable electron-withdrawing motifs could construct efficient D–π–A type polymer donors, such as PM6,[22] D18,[23] PTQ10,[24] PBTz-F,[25] and PBQx-F,[26] leading to enhanced power conversion efficiency (PCE) of NF-PSCs. These electron-accepting monomers influence not only the light-absorption properties and energy levels but also the formation of polymer donor films.[27,28] Thus, modifying electron-accepting monomers can help develop high-performance polymer donors.

Side-chain engineering, including the use of aromatic rings as side-chains and modification of π-bridge side-chains, is one of the commonly employed strategies for optimizing photovoltaic performance owing to side chains that have proven effective for fine-tuning the optoelectronic, molecular aggregation, charge mobility, and miscibility with non-fullerene acceptors.[29–32] Hou's group reported that replacing alkoxyl groups with aromatic substituents (alkylthienyl or alkylphenyl groups) in benzodithiophene (BDT) units significantly optimised the photovoltaic properties of

[a] *Northeast Guangdong Key Laboratory of New Functional Materials, Guangdong Rare Earth Photofunctional Materials Engineering Technology Research Center, School of Chemistry and Environment, Jiaying University, Meizhou, 514015, P. R. China. E-mail: liuyanjd2013@163.com, cgt_jy@126.com*

[b] *College of Chemistry, Key Lab of Environment-Friendly Chemistry and Application (Ministry of Education), Xiangtan University, Xiangtan 411105, P. R. China. E-mail: xiaomj7425@xtu.edu.cn*

† Electronic supplementary information (ESI) available. See DOI: https://doi.org/10.1039/d4ma01259c

‡ These authors contributed equally.

polymer donors.[33] Yan's, Hou's, Bo's, and Li's groups highlighted the influence of aromatic ring side-chains on the interchain/intermolecular stacking properties and photovoltaic performance of non-fullerene small-molecule acceptors, resulting in impressive PCEs.[34–37] Duan *et al.* and Yang *et al.* reported that the side-chains on the thiophene π-bridge affect the intermolecular interactions, charge transport, and active-layer morphology.[38,39] The benzodithiophenedione (BDD) unit is extensively used as an electron-deficient unit for constructing high-performance polymer donors, such as PBDB-T, PM6, owing to its quinoidal character, which enhances ICT effects.[17,40–42] Chen's group and our group reported that using the phenyl-substituted benzodithiophenedione (BDD-Ph) unit as a central core could construct efficient non-fused ring non-fullerene acceptors because the insertion of an aromatic substituent into a BDD unit could effectively enhance molecule aggregation and intermolecular stacking, thus improving the photovoltaic performance.[43,44] This suggests that using BDD-Ph as the electron-deficient unit and tailoring π-bridge side-chains may provide a pathway for developing an efficient WBG polymer donor.

In this work, we designed two novel copolymers, PBF-C8 and PBF-EH, with linear alkyl chains (*n*-octyl) or branched alkyl chains (2-ethylhexyl) on the thiophene π-bridge, respectively. These copolymers incorporated BDD-Ph and BDT as the electron-deficient and electron-donor units, respectively. Density functional theory (DFT) calculations indicated good backbone coplanarity of both copolymers. PBF-C8, with linear side-chains, exhibited red-shifted absorption and stronger molecular aggregation compared with PBF-EH. When paired with the narrow-bandgap non-fullerene acceptor L8-BO, PBF-C8-based devices achieved a PCE of 16.44%, higher than that of PBF-EH-based devices (3.21%). The superior performance of the PBF-C8:L8-BO configuration is attributable to enhanced carrier mobilities, exciton dissociation, and face-on orientation packing morphology. These results suggest that using the BDD-Ph unit as the electron-accepting unit, combined with tailored alkyl side-chains, is an effective strategy for constructing efficient polymer donors.

Results and discussion

Synthesis and characterization

Fig. 2 shows the synthesis pathways for PBF-C8 and PBF-EH, with detailed procedures outlined in the ESI† (Fig. S1–S5). PBF-C8 was synthesised through the Stille coupling reaction of compounds M6 and M8, while PBF-EH was obtained by copolymerising compounds M7 and M8. The number-average molecular weights (M_n) of PBF-C8 and PBF-EH were 73.5 and 89.4 kDa, respectively, with polydispersity indices of 2.15 and 2.07, as measured using high-temperature gel permeation chromatography. Thermogravimetric analysis (Fig. S6, ESI†) showed that the onset decomposition temperatures at 5% weight loss were 383 and 392 °C for PBF-C8 and PBF-EH, respectively, indicating exceptional thermal stability.[7,10] Moreover, the differential scanning calorimetry (DSC) measurement showed that no obvious melting and crystallization peaks could be found during the heating/cooling scans, implying that both copolymers exhibited low crystallization tendency (Fig. S7, ESI†).

Photophysical and electrochemical properties

Ultraviolet-visible (UV-vis) absorption spectra of PBF-C8 and PBF-EH were recorded in dilute $CHCl_3$ solution and solid films (Fig. 3), and the key data are presented in Table 1. In the solution, the short wavelength range near 350 nm was associated with the π–π* transitions of the copolymer backbones. The absorption peak at longer wavelengths was associated with ICT.[14] The maximum absorption peak of PBF-EH was located at 512 nm, while that for PBF-C8 was red shifted by 48 to 560 nm. PBF-C8 exhibited greater red shift than PBF-EH, implying that PBF-C8 with linear alkyl chains displayed stronger intermolecular π–π interactions and

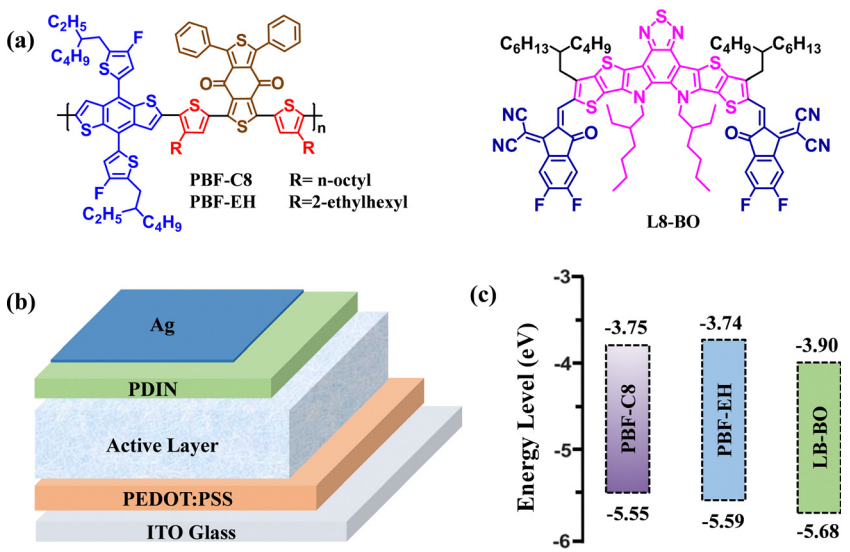

Fig. 1 (a) Chemical structures of PBF-C8, PBF-EH, and L8-BO. (b) Configuration of NF-PSCs. (c) Energy-level of PBF-C8, PBF-EH, and L8-BO.

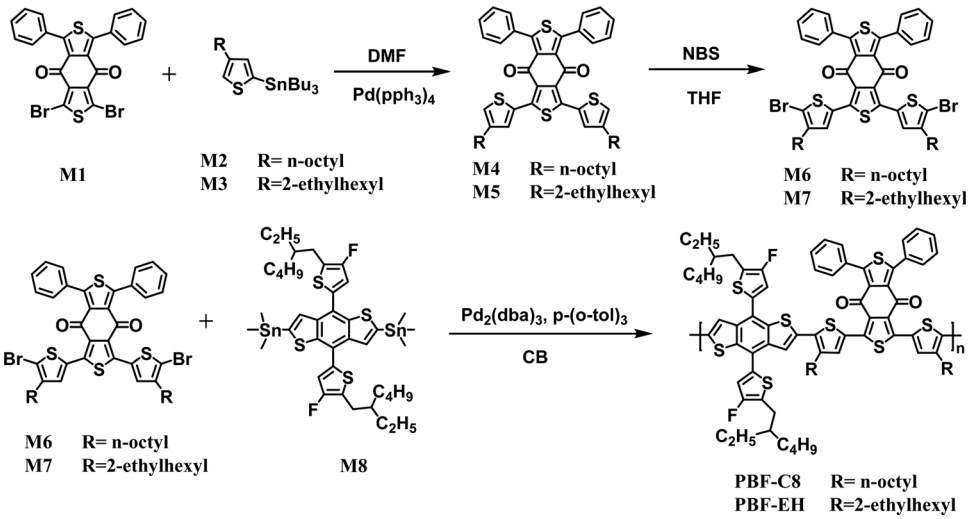

Fig. 2 Synthetic routes of PBF-C8 and PBF-EH.

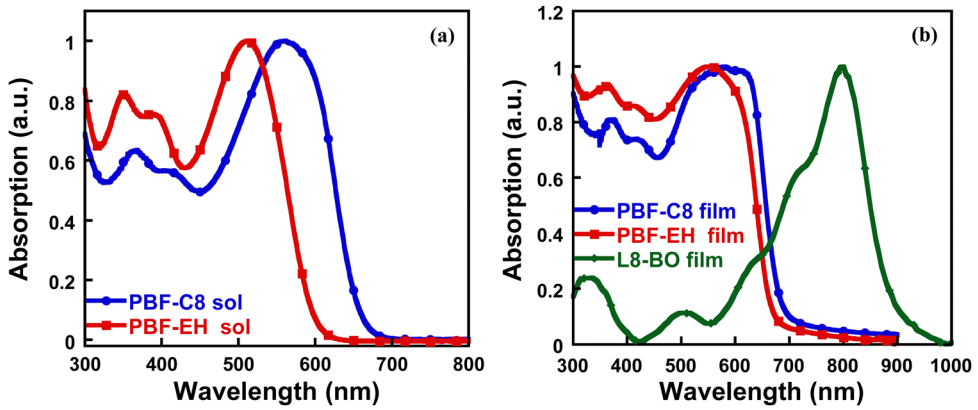

Fig. 3 (a) Absorption spectra of PBF-C8 and PBF-EH in $CHCl_3$ solution and (b) absorption spectra of PBF-C8, PBF-EH and L8-BO in thin films.

Table 1 Molecular weight, optical and electrochemical properties of PBF-C8 and PBF-EH

Copolymers	M_n (kDa)	PDI	λ_{max}^{sol} (nm)	λ_{max}^{film} (nm)	$E_g^{opt\,a}$ (eV)	E_{HOMO} (eV)	$E_{LUMO}{}^{b}$ (eV)	E_g (eV)
PBF-C8	73.5	2.15	560	581	1.80	−5.55	−3.75	1.80
PBF-EH	89.4	2.07	512	552	1.85	−5.59	−3.74	1.85

[a] E_g^{opt} values were calculated from the film absorption onsets. [b] E_{LUMO} calculated using E_{HOMO} and corresponding optical bandgap: $E_{LUMO} = E_{HOMO} + E_g^{opt}$.

demonstrating that linear alkyl chains were conducive to promoting aggregation. In neat films, the maximum absorption peaks (λ_{max}^{film}) of PBF-C8 and PBF-EH exhibited red shifts, appearing at 581 and 552 nm, respectively. PBF-EH exhibited a significant red-shift of 40 nm at longer wavelengths, whereas the red-shift observed for PBF-C8 is relatively minor owing to stronger aggregation behavior for PBF-C8 existing in solution.[45] Moreover, PBF-C8 displayed a noticeable shoulder peak, indicating stronger intermolecular aggregation compared with PBF-EH. The copolymer aggregation contributes to enhancing the absorption coefficients of PBF-EH and PBF-C8 from 4.35×10^4 to 7.63×10^4 cm^{-1} (Fig. S8, ESI†), which is beneficial to improve light-harvesting ability. The calculated optical band gaps for PBF-C8 and PBF-EH were 1.80 and 1.85 eV, respectively, based on the film absorption onsets. To further investigate the aggregations properties of the copolymers, the temperature-dependent absorption spectra of both copolymers in chlorobenzene solution were performed (Fig. S9, ESI†). As the temperature increases, PBF-C8 displays more pronounced blue-shifting characteristics than PBF-EH, indicating that PBF-C8 possessed a stronger aggregation behavior and the linear alkyl chains can enhance intermolecular π–π interactions.[18,31]

Cyclic voltammetry was performed to evaluate the electrochemical properties of PBF-C8 and PBF-EH (Fig. S10, ESI†), and their energy diagram is presented in Fig. 1c.[46] E_{HOMO} and E_{LUMO} were calculated as $E_{HOMO} = -e(E_{ox} + 4.80 - E_{Fc/Fc^+})$ and $E_{LUMO} = E_{HOMO} + E_g^{opt}$, respectively. The onset oxidation (E_{ox}) potentials were 1.16 and 1.21 V for PBF-C8 and PBF-EH, respectively. Thus, the $E_{HOMO/LUMO}$ of PBF-C8 and PBF-EH were −5.55/−3.75 and −5.59/−3.74 eV, respectively. Moreover, the E_{HOMO} and E_{LUMO} values of the L8-BO were −5.68 and −3.90 eV, respectively. Therefore, sufficient energy-level offsets existed between the donor and acceptor, which

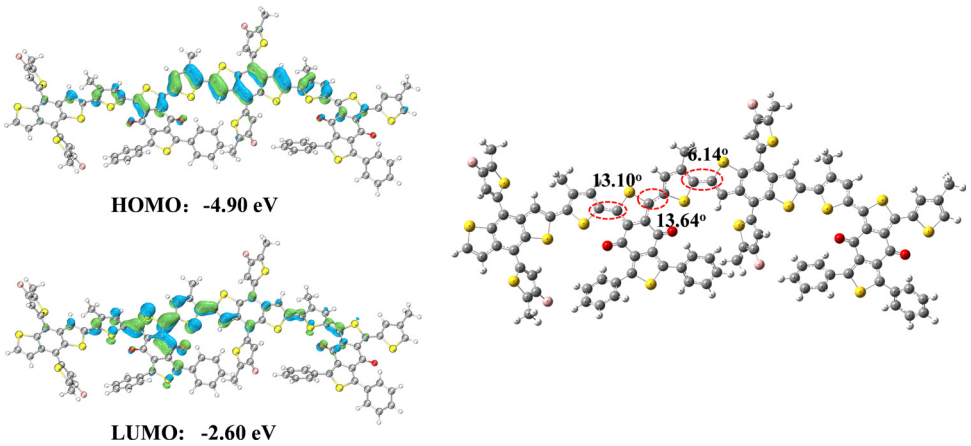

Fig. 4 Frontier molecular orbital surfaces and optimised molecular geometries for copolymers.

could promote efficient charge separation in NF-PSCs with PBF-C8 or PBF-EH as the donor and L8-BO as the acceptor.

Theoretical calculations

DFT calculations were conducted at the B3LYP level with the 6-31G* basis set to analyse the electronic properties and optimal geometries of the copolymers.[18] All alkyl chains were replaced with methyl groups in order to simplify the calculations. Since copolymers PBF-C8 and PBF-EH possessed the same conjugated backbone, the calculated dimers of both copolymers were also the same. As shown in Fig. 4, both PBF-C8 and PBF-EH exhibited well-distributed HOMO surfaces over the entire conjugated chain, while LUMO surfaces were primarily concentrated on the BDD-Ph unit (Fig. 4). This distribution indicated effective charge transport between the acceptor and donor motifs. PBF-C8 and PBF-EH displayed dihedral angles of 13.10° and 13.64° between BDD-Ph and thiophene unit, respectively, while the angles between the thiophene and BDT units were 6.14°. Thus, PBF-C8 and PBF-EH demonstrated a planar backbone, which can facilitate molecular stacking and charge transport.

Photovoltaic properties

To explore the influence of π-bridge alkyl side-chains on the photovoltaic performance, NF-PSCs were fabricated in the configuration ITO/PEDOT:PSS/copolymer:L8-BO/PDIN/Ag. The well-known fused-ring electron acceptor L8-BO was used as the acceptor, and the photovoltaic efficiencies of the NF-PSCs were optimised by modifying the donor/acceptor weight ratio, spin-coating speed, solvent additives, and annealing temperature for the PBF-C8:L8-BO blended film (Fig. S11–S14 and Tables S1–S5, ESI†). Optimal photovoltaic performance was achieved with a D/A weight ratio of 1 : 1.2, solution concentration of 16.5 mg mL^{-1} in $CHCl_3$ with 0.25% vol DIO as an additive, spin-coating speed of 1400 rpm, and thermal-annealing temperature of 100 °C. The PBF-C8:L8-BO-based device offered the highest PCE of 16.44%, with a V_{OC} of 0.915 V, a J_{SC} of 25.61 mA cm^{-2}, and an FF of 70.14%. In contrast, the PBF-EH-based device achieved a lower PCE of 3.21% owing to low J_{SC} and FF. The *J*–*V* characteristics of the optimal devices are presented in Fig. 5a, and the corresponding photovoltaic parameters are listed in Table 2.

External quantum efficiency (EQE) spectra (Fig. 5b) of the optimal NF-PSCs displayed photo-responses at wavelengths of 300–900 nm. The PBF-C8:L8-BO configuration exhibited enhanced EQE responses compared with PBF-EH:L8-BO, indicating more efficient charge generation and collection. Moreover, the EQE values of the PBF-C8:L8-BO-based device exceeded 80% at 500–800 nm. The integrated current densities were 25.40 and 8.58 mA cm^{-2} for PBF-C8:L8-BO- and PBF-EH:L8-BO-based

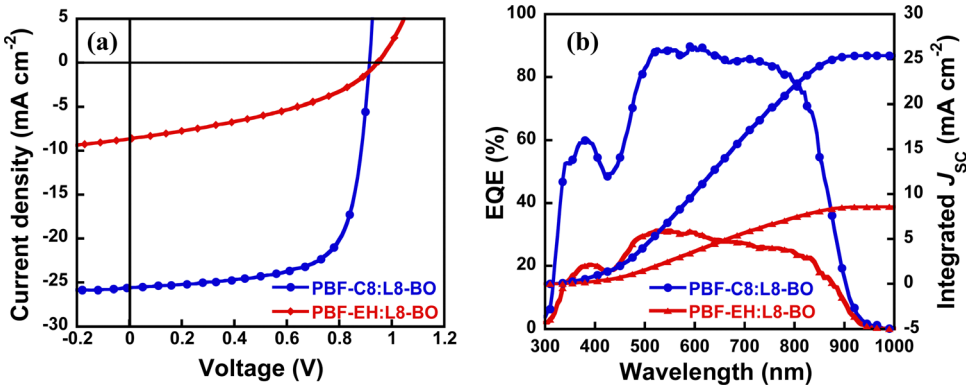

Fig. 5 (a) *J*–*V* characteristics and (b) EQE curves of the optimal devices.

Table 2 Photovoltaic parameters for PBF-C8- and PBF-EH-based devices

Devices	V_{OC} (V)	J_{SC} (mA cm^{-2})	$J_{SC(Calc)}$[a] (mA cm^{-2})	FF (%)	PCE[b] (%)
PBF-C8:L8-BO	0.915 (0.910 ± 0)	25.61 (25.54 ± 0.35)	25.4	70.14 (69.47 ± 1.62)	16.44 (16.15 ± 0.23)
PBF-EH:L8-BO	0.946 (0.940 ± 0.01)	8.65 (8.50 ± 0.30)	8.58	39.26 (38.22 ± 1.13)	3.21 (3.06 ± 0.11)

[a] Calculated from EQE spectra. [b] Statistical values were obtained from 10 independent NF-PSCs.

devices, respectively, consistent with the values obtained from the *J*–*V* curves.

Moreover, the long-term device stability of NF-PSCs in storage is very important to the practical application. The device stability of PBF-C8:L8-BO-based NF-PSCs was evaluated by heating the device at 60 °C in an N_2-filled glove box for 200 h (Fig. S15 and Table S6, ESI†). It is noted that the device retains ~81% of its initial PCE after 200 h storage. This result implies that PBF-C8:L8-BO-based NF-PSCs displayed a fair device stability.

Charge generation, transport, and recombination

To gain insights into the exciton dissociation properties of both devices, we measured the photocurrent density (J_{ph}) as a function of the effective voltage (V_{eff}) for the optimal devices (Fig. 6 and Tables S7, ESI†).[47] At V_{eff} = 2 V, both devices reached their saturated photocurrent density (J_{sat}), indicating that the photogenerated excitons were separated into free charges and collected by the electrodes without recombination. Theoretically, the exciton dissociation probability $P(E, T)$ can be calculated by normalising J_{ph} with J_{sat} under short-circuit conditions. The PBF-C8:L8-BO-based device exhibited a $P(E, T)$ of 92.04%, higher than that (76.53%) of the PBF-EH:L8-BO-based device. Thus, the PBF-C8:L8-BO-based device exhibited more efficient exciton dissociation properties than the PBF-EH:L8-BO-based device, contributing to its higher J_{SC} and FF.

The charge-carrier mobilities of neat copolymers and the optimal blend films were determined using the space-charge-limited current method to assess the influence of the alkyl side-chain topology on charge transport (Fig. S16 and S17, ESI†).[48]

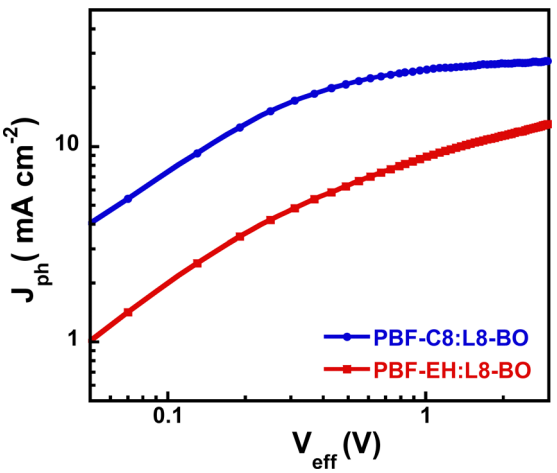

Fig. 6 J_{ph}–V_{eff} curves of the optimised devices based on PBF-C8 and PBF-EH.

As indicated in Table 3, the hole mobility of pure copolymer donor PBF-C8 film was 4.91 × 10^{-4} cm^2 V^{-1} s^{-1}, higher than that of PBF-EH film (2.58 × 10^{-4} cm^2 V^{-1} s^{-1}), which can be attributed to the improved intermolecular interactions and pronounced molecular stacking of PBF-C8 with linear side chains. The hole mobility (μ_h) of the PBF-C8:L8-BO-based blended film was 3.54 × 10^{-4} cm^2 V^{-1} s^{-1}, 4.78 times to that of the PBF-EH:L8-BO-based blended film (0.74 × 10^{-4} cm^2 V^{-1} s^{-1}). The superior μ_h for PBF-C8-based device was mainly ascribed to the stronger intermolecular interactions between PBF-C8 and acceptor induced by the intimate aggregation properties, as evidenced by the temperature-dependent absorption spectra of both copolymers (Fig. S9, ESI†). Similarly, the electron mobility (μ_e) of the PBF-C8:L8-BO-based blended film (3.47 × 10^{-4} cm^2 V^{-1} s^{-1}) exceeded that of the PBF-EH:L8-BO-based blended film (0.66 × 10^{-4} cm^2 V^{-1} s^{-1}). The PBF-C8:L8-BO-based device exhibited higher and more balanced carrier mobilities (μ_h/μ_e = 1.02) than the PBF-EH:L8-BO-based device (μ_h/μ_e = 1.12), which was beneficial to suppress space charge trapping and improve charge extraction, leading to enhanced J_{SC} and FF.[16] Thus, the PBF-C8:L8-BO-based device significantly outperforms the PBF-EH:L8-BO-based device.

Carrier recombination in PBF-C8- and PBF-EH-based devices was explored by examining the dependence of J_{SC} and V_{OC} on the light intensity (P_{light}). The relationship between P_{light} and J_{SC} can be expressed as $J_{SC} \propto (P_{light})^S$, where an S value close to 1 indicates negligible charge recombination.[49] The fitted S values for PBF-C8:L8-BO- and PBF-EH:L8-BO-based devices were 0.974 and 0.817, respectively (Fig. 7a), revealing less carrier recombination for the PBF-C8:L8-BO-based device, consistent with its improved J_{SC} and FF. The relationship between V_{OC} and P_{light} can be described as $V_{OC} \propto (nk_BT/q)\ln(P_{light})$, where k_B is the Boltzmann constant, q is the elementary charge, and T is the temperature. The slope (n) extracted from the fitting curves indicates the degrees of trap-assisted recombination. As shown in Fig. 7b, the slopes for the PBF-C8:L8-BO- and PBF-EH:L8-BO-based devices were 1.06 and 1.10 k_BT/q, respectively, confirming that the PBF-C8:L8-BO-based device exhibited less trap-assisted recombination.[50] Consequently, benefiting from the low carrier recombination and trap-assistant recombination observed in the above results, the device based on PBF-C8 finally obtains improved J_{SC} and FF than the PBF-EH-based device. These results

Table 3 Carrier mobilities of copolymer: L8-BO-based devices

Blended film	μ_h (cm^2 V^{-1} s^{-1})	μ_e (cm^2 V^{-1} s^{-1})	μ_h/μ_e
PBF-C8:L8-BO	3.54 × 10^{-4}	3.47 × 10^{-4}	1.02
PBF-EH:L8-BO	0.74 × 10^{-4}	0.66 × 10^{-4}	1.12

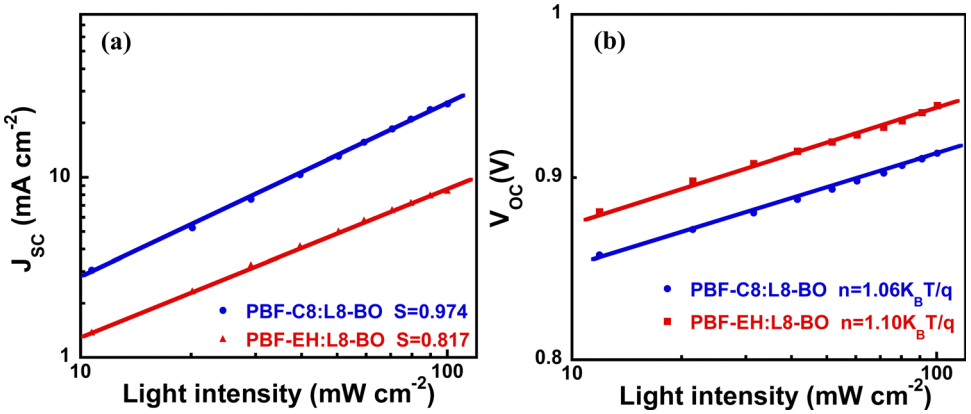

Fig. 7 P_{light} *vs.* (a) J_{SC} and (b) V_{OC} curves of PBF-C8 and PBF-EH-based devices.

Table 4 Charge generation and recombination of copolymer: L8-BO-based devices

Blended film	$P(E, T)$ (%)	S values	n
PBF-C8:L8-BO	92.04	0.974	$1.06k_BT/q$
PBF-EH:L8-BO	76.53	0.817	$1.10k_BT/q$

may be ascribed to the favorable face-on molecular orientation of PBF-C8, resulting in decreased recombination loss (Table 4).

Morphological investigation

To clarify the influence of alkyl side-chains on device performance, atomic force microscopy (AFM) and transmission electron microscopy (TEM) analyses were performed. As depicted in Fig. 8a and b, the PBF-C8:L8-BO blended film exhibited smoother surface morphologies with root mean square values of 1.53 nm, smaller than that of the PBF-EH:L8-BO film (3.30 nm). This enhanced miscibility facilitated exciton diffusion and charge transport, leading to higher J_{SC} and FF.[38,51] The TEM analysis provided insights into the bulk morphology of the optimal blended films (Fig. 8c and d). The PBF-C8:L8-BO film exhibited suitable phase separation with fibrillary networks, indicating good compatibility with the acceptor. Conversely, because PBF-EH showed poor compatibility with L8-BO, the PBF-EH:L8-BO film exhibited large-scale phase separation and displayed larger aggregate domain sizes. Thus, the PBF-C8:L8-BO-based blended film possessed a more favourable morphology, contributing to exciton splitting and thus improving the J_{SC} of the corresponding NF-PSCs.

The molecular packing of PBF-C8 and PBF-EH neat and blended films was evaluated through grazing-incidence wide-angle X-ray scattering (GIWAXS). Fig. 9a and b present the 2D GIWAXS patterns and 1D line-cut curves. The neat films of PBF-C8 and PBF-EH displayed a face-on orientation with sharp (010) π–π peaks at 1.59 and 1.56 Å^{-1} in the out-of-plane (OOP) direction and (100) lamellar peaks at 0.28 and 0.32 Å^{-1} in the in-plane (IP) direction. The π–π stacking distance of PBF-C8 in the OOP direction (3.949 Å) was smaller than that of PBF-EH (4.025 Å), suggesting more ordered face-on orientation for PBF-C8. Both blended films exhibited similar stacking features to their corresponding pure films. The PBF-EH:L8-BO film exhibited (010) refection peaks at 1.70 Å^{-1} in the OOP direction, with the (100) peaks located at 0.30 Å^{-1} in the IP direction and a (010) *d*-spacing of 3.694 Å. The PBF-C8:L8-BO film exhibited (010) refection peaks at 1.77 Å^{-1} in the OOP direction, with the (100) peaks located at 0.33 Å^{-1} in the IP direction and a (010) d-spacing of 3.548 Å. These results suggest that the stronger face-on stacking orientation of PBF-C8:L8-BO promotes vertical charge transportation, resulting in superior device performance.

Conclusions

We synthesised two novel copolymers, PBF-C8 with *n*-octyl alkyl chains and PBF-EH with 2-ethylhexyl alkyl chains on the thiophene π bridge, featuring BDD-Ph and BDT units as the electron acceptor and donor, respectively. PBF-C8 exhibited red-shifted absorption and stronger face-on stacking orientation than PBF-EH. When

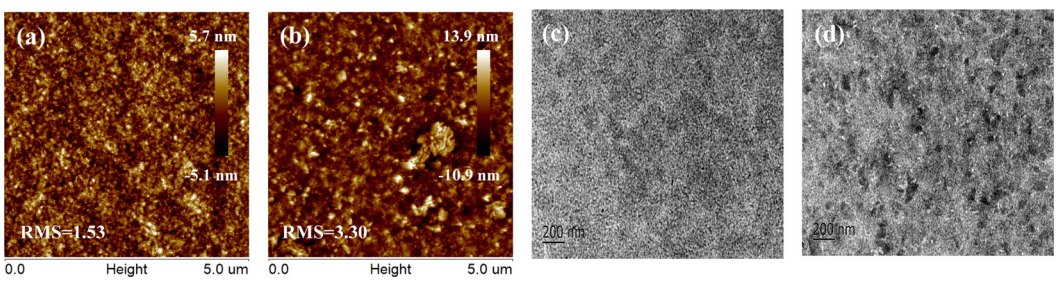

Fig. 8 (a) and (b) AFM height images and (c) and (d) TEM images of (a) and (c) PBF-C8:L8-BO- and (b) and (d) PBF-EH:L8-BO-based blended films.

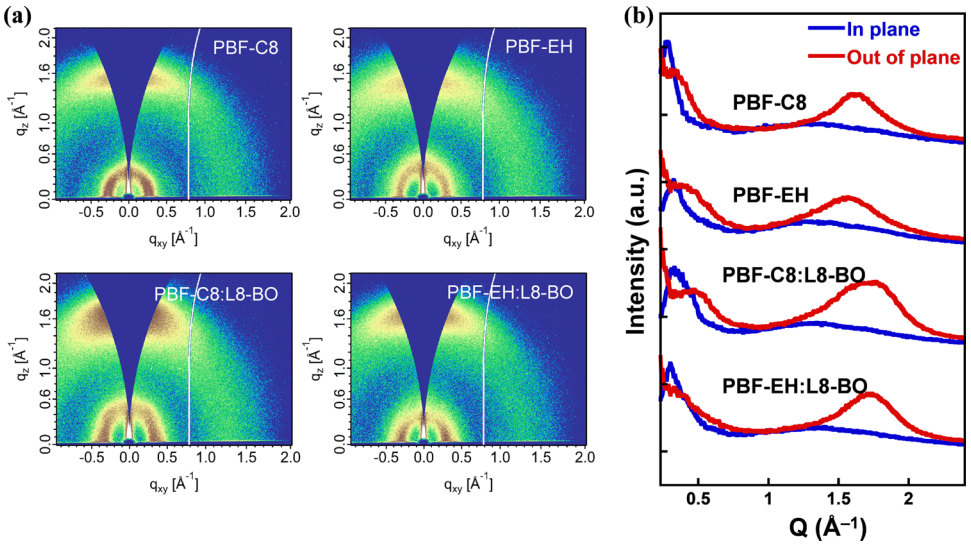

Fig. 9 2D GIWAXS patterns (a) and line-cut profiles in the IP and OOP directions (b) for PBF-C8 and PBF-EH neat and blended films.

paired with the narrow-bandgap acceptor L8-BO, NF-PSCs based on PBF-C8:L8-BO achieved a high PCE of 16.44%, significantly outperforming PBF-EH:L8-BO (3.21%). The enhanced performance of PBF-C8:L8-BO was attributable to reduced bimolecular recombination, enhanced carrier mobilities, and favourable morphology. Thus, using BDD-Ph as an electron-deficient unit and side-chain engineering offer a promising strategy for fabricating polymer donors for efficient NF-PSCs.

Data availability

The data supporting this article have been included as part of the ESI.†

Conflicts of interest

The authors declare no competing financial interest.

Acknowledgements

This work was supported by the Scientific Research Project of Education Department of Hunan Province (23B0167), the University Key Laboratory of Guangdong (2024KSYS021), the University Engineering Technology Center of Guangdong (No. 2022GCZX007), and the Inorganic optical functional materials and application innovation team of Guangdong (No. 2023KCXTD033).

References

1 G. Yu, J. Gao, J. C. Hummelen, F. Wudl and A. J. Heeger, *Science*, 1995, **270**, 1789–1791.
2 F. Huang, Z. S. Bo, Y. H. Geng, X. H. Wang, L. X. Wang, Y. G. Ma, J. Hou, W. P. Hu, J. Pei, H. L. Dong, S. Wang, Z. Li, Z. G. Shuai, Y. F. Li and Y. Cao, *Acta. Polym. Sin.*, 2019, **10**, 988–1046.
3 K. Fukuda, K. Yu and T. Someya, *Adv. Energy Mater.*, 2020, **10**, 2000765.
4 J. Wang and X. Zhan, *Acc. Chem. Res.*, 2021, **54**, 132–143.
5 D. Luo, C. J. Brabec and A. K. K. Kyaw, *Nano Energy*, 2023, **114**, 108661.
6 L. Zhu, M. Zhang, J. Xu, C. Li, J. Yan, G. Zhou, W. Zhong, T. Hao, J. Song, X. Xue, Z. Zhou, R. Zeng, H. Zhu, C.-C. Chen, R. C. I. MacKenzie, Y. Zou, J. Nelson, Y. Zhang, Y. Sun and F. Liu, *Nat. Mater.*, 2022, **21**, 656–663.
7 S. Guan, Y. Li, C. Xu, N. Yin, C. Xu, C. Wang, M. Wang, Y. Xu, Q. Chen, D. Wang, L. Zuo and H. Chen, *Adv. Mater.*, 2024, **36**, 2400342.
8 T. Jia, Y. Luo, Y. Hai, T. Lin, X. Qin, R. Ma, K. Fan, A. A. Sergeev, T. A. P. Dela Peña, Y. Li, M. Li, K. S. Wong, G. Li, J. Wu, S. Liu and F. Huang, *Energy Environ. Sci.*, 2024, **17**, 8593–8608.
9 T. Lin, Y. Hai, Y. Luo, L. Feng, T. Jia, J. Wu, R. Ma, T. A. D. Peña, Y. Li, Z. Xing, M. Li, M. Wang, B. Xiao, K. S. Wong, S. Liu and G. Li, *Adv. Mater.*, 2024, **36**, 2312311.
10 Y. Li, Z. Ge, L. Mei, H. Ma, Y. Chen, X. Wang, J. Yu, G. Lu, R. Yang, X. K. Chen, S. Yin and Y. Sun, *Angew. Chem., Int. Ed.*, 2024, **63**, e202411044.
11 X. Kong, N. Yang, X. Zhang, J. Zhang, Z. Li, X. Li, Y. Wu, R. Sun, J. Li, A. Li, J. Min, G. Yang and C. Sun, *Energy Environ. Sci.*, 2025, **18**, 386–396.
12 F. Yi, M. Xiao, Y. Meng, H. Bai, Z. F. Yao, W. Gao, G. Qi, Z. Liang, C. Jin, L. Tang, W. Su, R. Zhang, L. Yan, Y. Liu, W. Zhu, W. Ma and Q. Fan, *Angew. Chem., Int. Ed.*, 2024, **63**, e202319295.
13 M. Xiao, Y. Meng, L. Tang, P. Li, L. Tang, W. Zhang, B. Hu, F. Yi, T. Jia, J. Cao, C. Xu, G. Lu, X. Hao, W. Ma and Q. Fan, *Adv. Funct. Mater.*, 2024, **34**, 2311216.
14 Y. Li, H. Li, X. Xu, L. Yu, R. Li and Q. Peng, *Adv. Funct. Mater.*, 2025, DOI: **10.1002/adfm.202424327**.
15 S. Guan, Y. Li, C. Xu, N. Yin, C. Xu, C. Wang, M. Wang, Y. Xu, Q. Chen, D. Wang, L. Zuo and H. Chen, *Adv. Mater.*, 2024, **36**, 2400342.

16 H. Fu, Z. Wang and Y. Sun, *Angew. Chem., Int. Ed.*, 2019, **58**, 4442–4453.
17 J. Jin, Q. Wang, K. Ma, W. Shen, L. A. Belfiore, X. Bao and J. Tang, *Adv. Funct. Mater.*, 2023, **33**, 2213324.
18 J. Xu, H. Feng, Y. Liang, H. Tang, Y. Tang, Z. Du, Z. Hu, F. Huang and Y. Cao, *J. Energy Chem.*, 2022, **66**, 382–389.
19 H. Zhou, L. Yang and W. You, *Macromolecules*, 2012, **45**, 607.
20 Z. Li, C.-C. Chueh and A. K.-Y. Jen, *Prog. Polym. Sci.*, 2019, **99**, 101175.
21 Z. Cao, S. A. Tolba, Z. Li, G. T. Mason, Y. Wang, C. Do, S. RondeauGagné, W. Xia and X. Gu, *Adv. Mater.*, 2023, **35**, 2302178.
22 M. Zhang, X. Guo, W. Ma, H. Ade and J. Hou, *Adv. Mater.*, 2015, **27**, 4655.
23 Q. Liu, Y. Jiang, K. Jin, J. Qin, J. Xu, W. Li, J. Xiong, J. Liu, Z. Xiao, K. Sun, S. Yang, X. Zhang and L. Ding, *Sci. Bull.*, 2020, **65**, 272.
24 C. Sun, F. Pan, H. Bin, J. Zhang, L. Xue, B. Qiu, Z. Wei, Z.-G. Zhang and Y. Li, *Nat. Commun.*, 2018, **9**, 743.
25 B. Pang, C. Liao, X. Xu, L. Yu, R. Li and Q. Peng, *Adv. Mater.*, 2023, **23**, 2300631.
26 J. Wang, Y. Wang, P. Bi, Z. Chen, J. Qiao, J. Li, W. Wang, Z. Zheng, S. Zhang, X. Hao and J. Hou, *Adv. Mater.*, 2023, **35**, 2301583.
27 C. Zhu, K. Hu, L. Meng, X. Kong, W. Lai, S. Qin, B. Qiu, J. Zhang, Z. Zhang, Y. Wu, X. Li and Y. Li, *CCS Chem.*, 2023, **5**, 2378–2388.
28 G. Zhang, H. Ning, H. Chen, Q. Jiang, J. Jiang, P. Han, L. Dang, M. Xu, M. Shao, F. He and Q. Wu, *Joule*, 2021, **5**, 931–944.
29 P. Wan, C. An, T. Zhang, K. Ma, N. Liang, Y. Xu, S. Zhang, B. Xu, J. Zhang and J. Hou, *Polym. Chem.*, 2020, **11**, 1629–1636.
30 X. Dong, K. Yang, H. Tang, D. Hu, S. Chen, J. Zhang, Z. Kan, T. Duan, C. Hu, X. Dai, Z. Xiao, K. Sun and S. Lu, *Solar RRL*, 2019, **4**, 1900326.
31 H. Li, W. Yang, W. Wang, Y. Wu, T. Wang and J. Min, *Dyes Pigm.*, 2020, **186**, 108987.
32 W. Chen, G. Huang, X. Li, H. Wang, Y. Li, H. Jiang, N. Zheng and R. Yang, *ACS Appl. Mater. Interfaces*, 2018, **10**, 42747–42755.
33 L. Ye, S. Zhang, L. Huo, M. Zhang and J. Hou, *Acc. Chem. Res.*, 2014, **47**, 1595–1603.
34 G. Chai, Y. Chang, J. Zhang, X. Xu, L. Yu, X. Zou, X. Li, Y. Chen, S. Luo, B. Liu, F. Bai, Z. Luo, H. Yu, J. Liang, T. Liu, K. S. Wong, H. Zhou, Q. Peng and H. Yan, *Energy Environ. Sci.*, 2021, **14**, 3469–3479.
35 X. Kong, C. Zhu, J. Zhang, L. Meng, S. Qin, J. Zhang, J. Li, Z. Wei and Y. Li, *Energy Environ. Sci.*, 2022, **15**, 2011–2020.
36 L. Ma, S. Zhang, J. Zhu, J. Wang, J. Ren, J. Zhang and J. Hou, *Nat. Commun.*, 2021, **12**, 5093.
37 H. Lu, X. Wang, H. Wang, A. Zhang, X. Zheng, N. Yu, Z. Tang, X. Xu, Y. Liu, Y.-N. Chen and Z. Bo, *Sci. China: Chem.*, 2022, **65**, 594–601.
38 C. Duan, J. J. V. Franeker, M. M. Wienk and R. A. J. Janssen, *Polym. Chem.*, 2016, **7**, 5730–5738.
39 D. Zhu, X. Bao, Q. Zhu, C. Gu, M. Qiu, S. Wen, J. Wang, B. Shahid and R. Yang, *Energy Environ. Sci.*, 2017, **10**, 614–620.
40 D. Qian, L. Ye, M. Zhang, Y. Liang, L. Li, Y. Huang, X. Guo, S. Zhang, Z. Tan and J. Hou, *Macromolecules*, 2012, **45**, 9611–9617.
41 M. Xiao, L. Liu, Y. Meng, B. Fan, W. Su, C. Jin, L. Liao, F. Yi, C. Xu, R. Zhang, A. K.-Y. Jen, W. Ma and Q. Fan, *Sci. China: Chem.*, 2023, **66**, 1500–1510.
42 B. Zheng, L. Huo and Y. Li, *NPG Asia Mater.*, 2020, **12**, 3.
43 S. Deng, W. Luo, L. Zhang, G. Xie, S. Lei, M. Luo, Z. Wu, D. Yuan, J. Liang, Z. Xie and J. Chen, *J. Mater. Chem. A*, 2023, **11**, 3437–3445.
44 B. He, W. Zhang, J. Zhang, M. Xiao and G. Chen, *Synth. Met.*, 2024, **308**, 117716.
45 P. Chao, H. Chen, M. Pu, Y. Zhu, L. Han, N. Zheng, J. Zhou, X. Chang, D. Mo, Z. Xie, H. Meng and F. He, *Adv. Sci.*, 2021, **8**, 2003641.
46 E. Espinoza, J. Clark, J. Soliman, J. Derr, M. Morales and V. Vullev, *J. Electrochem. Soc.*, 2019, **166**, 3175–3187.
47 J. L. Wu, F. C. Chen, Y. S. Hsiao, F. C. Chien, P. Chen, C. H. Kuo, M. H. Huang and C. S. Hsu, *ACS Nano*, 2011, **5**, 959–967.
48 S. M. H. Rizvi and B. Mazhari, *J. Appl. Phys.*, 2017, **121**, 155501.
49 M. M. Mandoc, F. B. Kooistra, J. C. Hummelen, B. D. Boer and P. W. M. Blom, *Appl. Phys. Lett.*, 2007, **91**, 263505.
50 B. Fan, X. Du, F. Liu, W. Zhong, L. Ying, R. Xie, X. Tang, K. An, J. Xin, N. Li, W. Ma, C. J. Brabec, F. Huang and Y. Cao, *Nat. Energy*, 2018, **3**, 1051–1058.
51 T. Dai, A. Tang, Z. He, M. Du, P. Lei, Q. Zeng, Z. Wang, Y. Wang, S. Lu, Y. Zhong and E. Zhou, *Energy Environ. Sci.*, 2023, **16**, 2199–2211.